DOI: 10.48011/asba.v2i1.1319

A Robust Longitudinal Stability Augmentation System for Small Aircraft Under Parametric Uncertainty

Guilherme N. Barufaldi [*] **Marcus H. Victor Jr.** [**]
Henrique W. R. Pereira [**] **Roberto G. A. da Silva** [*]

[*] *Aeronautical Engineering Division, Instituto Tecnológico de Aeronáutica, SP, (e-mail: guilherme.barufaldi@protonmail.com).*
[**] *Electronics Engineering Division, Instituto Tecnológico de Aeronáutica, SP.*

Abstract: Small unmanned aerial vehicles (UAVs) face flying quality problems different from those encountered by larger aircraft. The lower airspeeds and small dimensions make these vehicles more susceptible to gusts and stability and control issues, which may render the aircraft difficult to fly. Moreover, due to many factors, UAVs are often built with a considerable degree of uncertainty regarding their aerodynamic properties and flying quality. The resulting aircraft may present poor stability and handling characteristics. This work presents the conceptual design of a robust stability augmentation system (SAS), aimed at increasing stability characteristics and protecting aircraft prone to flying quality problems. In order to deal with parametric uncertainties, the controller was designed with the robust H_∞ technique. The design process is presented, and a parametric aircraft model is provided, together with longitudinal stability and control derivatives. Simulations are presented to show the effects of the controller on the aircraft behavior.

Keywords: unmanned aerial vehicles, flight control, flight dynamics, robust control, stability augmentation system

1. INTRODUCTION

The unmanned aerial vehicles (UAV) market is booming, currently occupying a significant area of aeronautical research and development. The evolution of control theory and flight computers, and the miniaturization of electronic components have fostered the progress of small remotely-controlled or autonomous aircraft.

A significant percentage of UAVs is made up of relatively small vehicles, often launched by hand. These smaller aircraft face flying quality problems different from those encountered by larger vehicles. The smaller dimensions and particular flight regime, which often occurs at low speeds, make these airplanes more susceptible to gusts and stability and control issues, such as higher natural frequencies or higher sensitivity to control inputs (Peters and Andrisani, 1997).

Most small UAVs have to carry payloads that are bulky and heavy when compared to the aircraft size and its gross takeoff weight. Therefore, due to scale factors, the designs of these vehicles have to incorporate less conservative and sometimes unorthodox solutions to meet the desired performance and payload requirements. Since these vehicles do not carry any lives on board, these less conventional solutions are not a problem. However, unwanted effects on handling may appear (Keane et al., 2017).

Many small companies and research institutes that conduct UAV design and development operate with relatively low budgets and do not have access to wind tunnels. Therefore, these institutions resort to computational aerodynamic tools, such as CFD (computational fluid dynamics) or panel method codes to design and analyze their products. Although useful, such tools do not always provide accurate data due to modeling or numerical limitations. As a result, many aircraft are built with a considerable degree of uncertainty regarding their aerodynamic characteristics.

One of the most important parameters provided by aerodynamic analysis is the position of the neutral point (NP), a fixed point in the body where the resultant aerodynamic force is placed such that the aerodynamic moment over the airplane is constant. The position of the NP is required to adjust the position of the center of gravity (CG), and the distance between the two points is critical to the airplane longitudinal stability and flying qualities (Nelson, 1989). This distance is usually expressed as a percentage of the mean aerodynamic chord of the wing (MAC) and is named static margin (SM).

Inaccuracies in the NP position result in incorrect static margin values, even with an accurate adjustment of the CG position. The issue, in this case, is that the real NP position is unknown and, therefore, the real SM value is also unknown. This poses a problem for the initial flight tests, when the aircraft is flown for the first time, and

[⋆] This study was financed by the Coordenação de Aperfeiçoamento de Pessoal de Nível Superior – Brasil (CAPES) – Finance Code 001.

the pilot and engineers still have to figure out how it will behave, and how sensitive it is.

Some aircraft configurations are quite sensitive to CG adjustments (Keane et al., 2017), especially those with low or zero horizontal tail volume, such as flying wings. Therefore, this uncertainty about the real SM value constitutes a serious issue and may result in accidents. Figure 1 shows a sequence of images where a prototype flying-wing UAV, developed at the Instituto Tecnológico de Aeronáutica for the SAE AeroDesign Brasil competition, crashes into the ground soon after takeoff.

In post-accident analyses, it was found that the aircraft in Fig. 1 presented poor longitudinal stability and was very sensitive to control surface deflections. A combination of excessive control inputs and mild turbulence caused the pilot to lose control, and the aircraft stalled at a low height. The pilot was unable to recover, and the aircraft crashed into the ground. The probable cause of the low stability was a combination between an inherently sensitive design and an incorrect SM value, lower than calculated from software data.

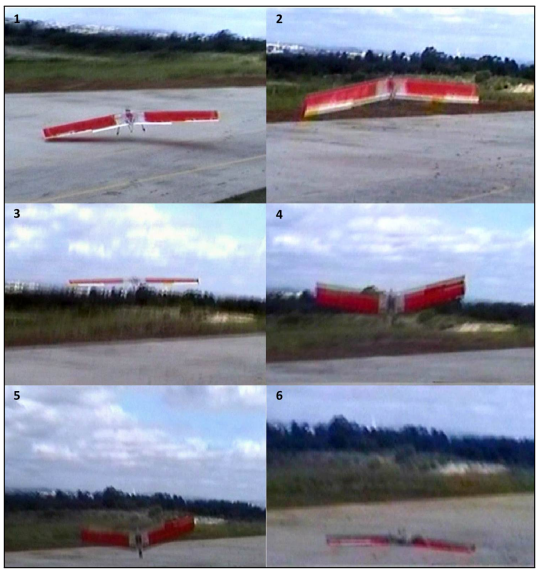

Figure 1. An accident with a prototype UAV, which took off with trim problems and crashed soon after. The images are numbered chronologically.

One possible solution to mitigate the problem of poor longitudinal stability and flying quality is to use a stability augmentation system (SAS). This control system combines the pilot inputs with the signal from a feedback controller designed to improve the dynamic response and stability characteristics of the airplane (Stevens and Lewis, 2003). However, in this case, the controller design must take into account the fact that some of the system parameters are not accurately known.

This work presents the conceptual design of a robust longitudinal stability augmentation system (SAS), aimed at increasing stability characteristics and protecting aircraft prone to longitudinal flying quality problems. In order to deal with parametric uncertainties, the controller design employs the robust H_∞ technique. With the intention of achieving reliability and cost-effectiveness, the system was designed with simplicity as the main guideline, and only one gyro is required for the feedback signal.

A similar approach is employed in (Kannan and Bhat, 2005), in which a robust longitudinal SAS is developed with the H_∞ technique. However, a more complex design is presented, with the full longitudinal dynamics and thrust vector control in a discrete-time framework. Lombaerts et al. (2005) developed a more complex robust control system for a UAV also employing the H_∞ technique. The control system acts on three axes and also incorporates a control augmentation system (CAS). However, the authors do not address flying quality improvements.

2. AIRCRAFT MODEL

In this section, the aerodynamic model, the longitudinal dynamic equations, the actuator dynamics, and the linearized system are presented.

2.1 Aerodynamic Model

The aerodynamic net force acting on the aircraft is divided into two components: the lift force L and the drag force D, as shown by (1) and (2), respectively.

$$L = \frac{\rho V^2}{2} S C_L \tag{1}$$

$$D = \frac{\rho V^2}{2} S C_D \tag{2}$$

where ρ is the air density; V is the velocity (true airspeed, or TAS); S is the wing planform area; C_L is the dimensionless lift coefficient; and C_D is the dimensionless drag coefficient. Both C_L and C_D are properties of the aircraft geometric form and both depend solely on the angle of attack α, if compressibility effects are negligible – these effects would only be significant for higher Mach numbers, which is not the case for propeller-driven UAVs. However, it is customary to express C_D as a function of C_L. Since the drag coefficient exhibits a parabolic behavior, a standard quadratic drag polar model is assumed, as shown by (3).

$$C_D = C_{D_0} + k \cdot C_L^2 \tag{3}$$

where C_{D_0} is the zero-lift drag coefficient, and k is the lift-dependent drag constant. Equation (4) shows C_L as an affine function of the angle of attack α.

$$C_L = C_{L_0} + C_{L_\alpha} \alpha \tag{4}$$

where C_{L_0} is the lift coefficient for zero angle of attack, and C_{L_α} is the derivative of C_L with respect to α.

The aerodynamic moment (M_A) around the CG is given by (5).

$$M_\mathrm{A} = \frac{\rho V^2}{2} \bar{c} S C_m \tag{5}$$

where $\bar{c}$ is the mean aerodynamic chord of the wing, and C_m is the dimensionless pitching moment coefficient. Equation (6) shows the linearized model to calculate C_m.

$$C_m = C_{m_0} + C_{m_\alpha}\alpha + C_{m_q}\frac{\bar{c}q}{2V_r} + C_{m_{\delta e}}\delta_e \tag{6}$$

where q is the pitch rate; δ_e is the elevator deflection; and V_r is a reference airspeed. The coefficients C_{m_0}, C_{m_α}, C_{m_q} and $C_{m_{\delta e}}$ are known as the stability and control derivatives (Etkin and Reid, 1996).

The static margin (SM) is defined by (7).

$$\mathrm{SM} = \frac{x_{\mathrm{NP}} - x_{\mathrm{CG}}}{\bar{c}} \tag{7}$$

where x_{NP} and x_{CG} are the positions of the NP and the CG, with respect to an arbitrary reference point (*datum*), respectively. The derivative C_{m_α} is a function of SM, and is given by (8).

$$C_{m_\alpha} = -C_{L_\alpha} \cdot \mathrm{SM} + C_{m_{\alpha,0}} \tag{8}$$

where $C_{m_{\alpha,0}}$ is a term independent of the static margin, and accounts for the contributions of the fuselage and the horizontal tail to C_{m_α}.

Another relevant figure to consider is the stall speed, the minimum airspeed with which the aircraft is able to maintain level flight. The stall speed V_s is calculated according to (9).

$$V_s = \sqrt{\frac{2W}{\rho S C_{L_{\max}}}} \tag{9}$$

where $C_{L_{\max}}$ is the maximum lift coefficient the aircraft can achieve and W is the aircraft weight.

2.2 Longitudinal Dynamics

The main goal of the robust SAS is to improve longitudinal flying qualities. Since the coupling between longitudinal and lateral-directional modes is weak, it can be neglected (Duke et al., 1988). Hence, the longitudinal dynamic model of the aircraft is sufficient, and it is represented by the following differential equations (Nelson, 1989).

$$\dot{V} = \left(\frac{g}{W}\right)(T\cos\alpha - D - W\sin\gamma) \tag{10}$$

$$\dot{\gamma} = \left(\frac{g}{WV}\right)(T\sin\alpha + L - W\cos\gamma) \tag{11}$$

$$\dot{\alpha} = q - \dot{\gamma} \tag{12}$$

$$\dot{q} = \frac{M_A}{I_{yy}} \tag{13}$$

where g is the acceleration of gravity; γ is the flightpath angle; W is the aircraft weight, assumed constant; T is the thrust force provided by the propeller; I_{yy} is the mass moment of inertia. Since small UAVs usually fly at low heights, the variation of air density ρ can be neglected and, therefore, there is no need to consider altitude variations.

The longitudinal dynamics of a fixed-wing aircraft are well known (Etkin and Reid, 1996), and there are two distinct oscillatory modes: a short period mode, with higher frequency and damping, and a long period mode (also known as phugoidal mode), with lower frequency and weak damping. Since the short period mode, described by state variables α and q is much more critical to control, and requires faster reactions from the pilot, the SAS is designed to improve characteristics of this mode only – it is assumed that the pilot can easily control phugoidal oscillations since it is a "slow" mode. Although both modes are coupled, the coupling can be neglected in the case of the short period mode, since the effects of the phugoidal mode on the short period are weak (Nelson, 1989).

2.3 Actuator dynamics

For conceptual design purposes, control surface actuators are commonly modeled as first-order systems, such as in (Stevens and Lewis, 2003). The elevator actuator transfer function $G_A(s)$, which relates the elevator deflection δ_e to control input u_e, is presented in (14).

$$G_A(s) = \frac{N_A}{s + D_A} \tag{14}$$

where N_A and D_A are actuator parameters, assumed constant. In this case, the elevator deflection becomes a state variable rather than a control input. The state-space differential equation representing the actuator dynamics is presented in (15).

$$\dot{\delta}_e = -D_A\,\delta_e + N_A\,u_e \tag{15}$$

2.4 Linearized Dynamical System

State-space model is a very useful representation for linear time-invariant (LTI) systems and can be represented as (16).

$$\begin{aligned} \dot{x}(t) &= A\,x(t) + B\,u(t) \\ y(t) &= C\,x(t) \end{aligned} \tag{16}$$

where t is the time, $x \in \mathbb{R}^n$ are the states, $u \in \mathbb{R}^m$ are the control inputs, and $y \in \mathbb{R}^p$ are the outputs. Model matrices have the following dimensions: $A \in \mathbb{R}^{n\times n}$, $B \in \mathbb{R}^{n\times m}$, and $C \in \mathbb{R}^{p\times n}$.

The longitudinal dynamic model expressed by (10) to (12) is nonlinear. The methods adopted for the controller design require a linear system, and hence a linearization procedure is applied, as shown in (17).

$$\dot{x}_{sp} = \underbrace{\begin{bmatrix} \frac{\partial f_1}{\partial \alpha} & \frac{\partial f_1}{\partial q} \\ \frac{\partial f_2}{\partial \alpha} & \frac{\partial f_2}{\partial q} \end{bmatrix}}_{A_{sp}} x_{sp} + \underbrace{\begin{bmatrix} \frac{\partial f_1}{\partial u} \\ \frac{\partial f_2}{\partial u} \end{bmatrix}}_{B_{sp}} \delta_e \tag{17}$$

where $x_{sp} = [\Delta\alpha \;\; \Delta q]^T$; and f_1 and f_2 are the scalar functions that return $\dot{\alpha}$ and $\dot{q}$, respectively – (12) and (13). The system described in (17) represents the short period (SP) approximation, which is the oscillatory mode improved by the SAS. As explained before, the SP mode is more critical to control, and involves the angle of attack, which has a critical limit known as stall angle, for which the C_L value is at a maximum. When α is increased beyond this limit, the lift coefficient decreases, and the aircraft is unable to sustain leveled flight. Therefore, it

is more critical to stabilize the SP mode. Moreover, the SP approximation yields good results and is sufficiently accurate to design a SAS (Stevens and Lewis, 2003).

The variations of the state variables around the point of interest $\mathbf{x}_0$ are calculated as shown in (18) and (19).

$$\Delta\alpha = \alpha - \alpha_0 \tag{18}$$
$$\Delta q = q - 0 = q \tag{19}$$

The partial derivatives of f_1 and f_2 shown in (17) are given by (20) to (25).

$$\frac{\partial f_1}{\partial \alpha} = -\left(\frac{g}{W}\right)\frac{\rho V_0^2 S C_{L_\alpha} + 2T_0 \cos\alpha_0}{2V_0} \tag{20}$$
$$\frac{\partial f_1}{\partial q} = 1 \tag{21}$$
$$\frac{\partial f_2}{\partial \alpha} = \frac{\rho V_0^2 \bar{c} S C_{m_\alpha}}{2I_{yy}} \tag{22}$$
$$\frac{\partial f_2}{\partial q} = \frac{\rho V_0^2 \bar{c}^2 S C_{m_q}}{4I_{yy}V_r} \tag{23}$$
$$\frac{\partial f_1}{\partial u} = 0 \tag{24}$$
$$\frac{\partial f_2}{\partial u} = \frac{\rho V_0^2 \bar{c} S C_{m_{\delta e}}}{2I_{yy}} \tag{25}$$

where V_0, α_0 and T_0 are the velocity, angle of attack and propeller thrust values at the point of interest in which the system is linearized, respectively.

The complete system, such as indicated in (16), is obtained by combining the the actuator differential equation (15) and the short period system (17). The complete linearized system is presented in (26).

$$\dot{x} = \underbrace{\left[\begin{array}{cc|c} & A_{sp} & B_{sp} \\ \hline 0 & 0 & -D_A \end{array}\right]}_{A} x + \underbrace{\begin{bmatrix} 0 \\ 0 \\ N_A \end{bmatrix}}_{B} u_e \tag{26}$$

where x is the complete state vector, such that $x = [\Delta\alpha\ \Delta q\ \Delta\delta_e]^T$; and u_e is the control input.

2.5 Example Aircraft and Parametric Uncertainties

In order to test the designed SAS, a small electric UAV was selected as a reference aircraft. This vehicle was originally developed for the Micro Class category of the SAE AeroDesign Brasil competition and has been employed as a testbed for experiments and flight tests. It has already been flown several times, and its behavior is well known. The actual airplane is shown in flight in Fig. 2.

Figure 2. The UAV used for the simulations, in flight.

The relevant parameters of geometry and inertia are given in Table 1, and the dimensionless aerodynamic coefficients [1] are given in Table 2. The actuator parameters are shown in Table 3.

Table 1. Aircraft geometric and inertial parameters.

Parameter	Value
Length – l	1100 mm
Wingspan – b	1400 mm
MAC – $\bar{c}$	230 mm
Wing planform area – S	0.322 m^2
Maximum takeoff weight – $W_{\max}$	20 N
Mass moment of inertia – I_{yy}	0.042 kg $\cdot$ m^2
$C_{L_{\max}}$	1.4

Table 2. Dimensionless stability and control derivatives, and relative uncertainties.

Coefficient	Value	Rel. uncertainty (%)
C_{L_α}	4.3863	$\pm$ 15
C_{L_0}	0.2092	0
C_{D_0}	0.0230	0
k	0.0703	0
C_{m_0}	0.0100	0
C_{m_α}	-0.5386	$\pm$ 30
C_{m_q}	-0.8280	$\pm$ 15
$C_{m_{\delta e}}$	-0.3840	$\pm$ 15

Table 3. Actuator parameters.

Parameter	Value
N_A	52.06
D_A	52.06

The uncertain variables are some of the dimensionless stability and control derivatives. The uncertainty ranges considered for each one of theses parameters are presented in Table 2 - coefficients with zero uncertainty do not impact the controller design. The relative uncertainties were set at 15%, and are superior to those commonly found in literature, e.g. (Jatengaokar, 2006), in order to account for the model inaccuracies explained in Sec. 1. To account for both parametric and static margin uncertainties, the relative uncertainty for C_{m_α} is set at 30%, twice as high. C_{m_α} is obtained from (8) but, for the sake of simplicity, the uncertainty is applied directly to its final value.

[1] The aerodynamic coefficients were calculated with the *Athena Vortex Lattice* program, available at: `http://web.mit.edu/drela/Public/web/avl/`.

3. CONTROL SYSTEM DESIGN

3.1 Basic Design Characteristics

The longitudinal SAS is a feedback control system designed to improve the airplane longitudinal stability characteristics. In this particular case, the main goal is to obtain a closed-loop system with increased damping in order to reduce oscillatory tendencies. Since this SAS is geared towards aircraft whose aerodynamic characteristics are not accurately known, it must be able to keep good performance for all the uncertainties considered in the model. In other words, the control system must be robust and, therefore, a robust control design technique is employed.

One design guideline commonly employed to increase system reliability is to keep the design as simple as possible. In this case, the control system acts only on one control surface, the elevator on the horizontal tail, and does not override pilot authority. Moreover, only one sensor is employed – a gyro – thus only one output is fed back to the controller – the pitch rate. This eliminates the need to measure or estimate the angle of attack, which is particularly difficult, especially for small aircraft (Stevens and Lewis, 2003). The robust SAS block diagram is shown in Fig. 3.

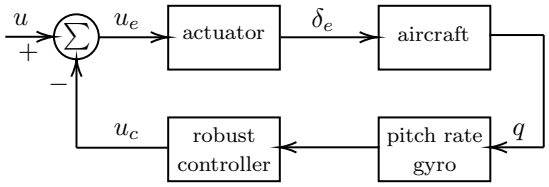

Figure 3. Robust longitudinal stability augmentation system block diagram.

3.2 Robust Controller Design

Robust controller methodologies are well suited for the stated problem, as such approaches can provide useful properties for the closed-loop system due to their inherent capabilities to handle model parameter uncertainties (Skogestad and Postlethwaite, 2007). The set of models described by all possible parameter ranges is dealt with at once, furnishing simplicity to the controller design (Zhou and Doyle, 1998).

Robust controller design using normalized coprime factor plant descriptions is a well-known design technique that aims to minimize the H_∞ norm. One of the H_∞ design techniques is the loop shaping where a coprime factorization is used on H_∞ minimization (McFarlane and Glover, 1990). This method considers nonparametric uncertainties to its synthesis and provides robust performance and stability to the closed-loop system. Our problem does not present this kind of uncertainty and this characteristics are not guaranteed, however robust performance is evaluated by time-domain simulations. Because of this consideration it is also important to note that the obtained results are conservative.

Considering the following plant realization (G), such that $G = M_l^{-1} N_l$:

$$G = \left[\begin{array}{c|c} A & B \\ \hline C & 0 \end{array}\right] \tag{27}$$

If the system is detectable, then there exists a coprime factorization such that $G = M_l^{-1} N_l$. These terms can be calculated as:

$$[M_l \quad N_l] = \left[\begin{array}{c|cc} A + HC & H & B \\ \hline C & I & 0 \end{array}\right] \tag{28}$$

where $H = -YC^T$ and Y is the solution of the Riccati equation (29):

$$AY + YA^T - YC^T CY + BB^T = 0 \tag{29}$$

The controller structure is given by (30).

$$K = \left[\begin{array}{c|c} A - BB^T X_\infty + HC & H \\ \hline -B^T X_\infty & 0 \end{array}\right] \tag{30}$$

where $X_\infty \geq 0$ is the stabilizing solution of the Riccati equation (31):

$$X_\infty \left(A + \frac{HC}{\psi^2 - 1}\right) + \left(A + \frac{HC}{\psi^2 - 1}\right)^T X_\infty - X_\infty \left(BB^T - \frac{HH^T}{\psi^2 - 1}\right) X_\infty + \frac{\psi^2 C^T C}{\psi^2 - 1} = 0 \tag{31}$$

The performance criterion ψ is greater than 1, and it can be calculated with:

$$\psi_{\min} = \frac{1}{\sqrt{1 - \lambda_{\max}(YQ)}} \tag{32}$$

where $\lambda_{\max}$ is the maximum eigenvalue and Q is the solution of the Lyapunov equation (33):

$$Q(A - YC^T C) + (A - YC^T C)Q + C^T C = 0 \tag{33}$$

4. RESULTS AND DISCUSSION

4.1 Robust Controller Design Procedure

The frequency response of the singular values of the nominal plant (G) is shown in Fig. 4. The response exhibits small gains in low and small declination in high frequencies. To improve performance, we used a loop shaping procedure, in which the shaped plant (G_s) is represented by $G_s = W_1 \cdot G \cdot W_2$. The design parameters W_1 and W_2 were tailored to achieve better performance in low and steeper declination in high frequencies (34).

$$\begin{aligned} W_1 &= \frac{1}{s} \\ W_2 &= 1 \end{aligned} \tag{34}$$

From Fig. 4, the desired plant (G_s) presents superior behavior in tracking (higher gains in low frequencies), and improved noise rejection (steeper declination in high frequencies).

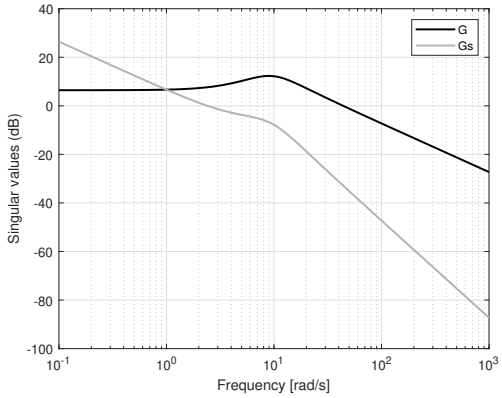

Figure 4. Singular value responses of nominal (G) and desired (G_s) plants.

By using equations from Section 3.2, we obtained the following controller transfer function:

$$K(s) = \frac{-2.3145(s^2 + 10.92s + 84.13)}{s(s + 3.111)(s^2 + 13.99s + 125)} \tag{35}$$

The singular values for the nominal plant are presented in Fig. 5, showing the open loop (L), the sensitive (S), and the complementary sensitive (T) functions, which are used to assess the system behavior with the designed controller. The frequency response of both S and T do not present peaks at any frequencies and have smooth shapes. In small frequencies, S presents small and L presents high gains, indicating that the plant exhibits good tracking and good disturbance rejection. In high frequencies, the frequency responses for T and L are very low, indicating that the plant have good noise rejection.

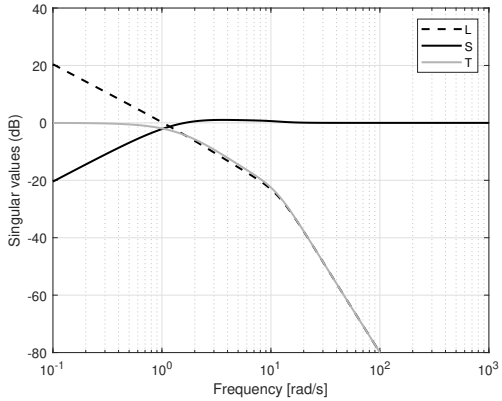

Figure 5. Nominal frequency responses of the singular values of open loop (L), sensitive (S), and complementary sensitive (T) functions.

Figure 6 presents the singular values of the sensitive function (S) and the complementary sensitive function (T), for all the possible plants comprising model uncertainties. The properties analysed in Fig. 5 hold for both low and high frequencies for all the possible plants. Moreover, S and T do not present high peaks in any frequencies and have smooth shapes.

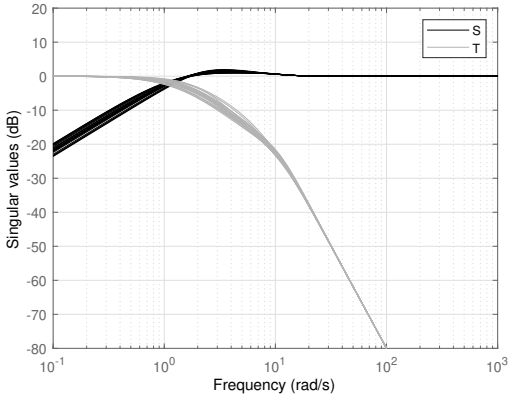

Figure 6. Frequency responses of the singular values of the sensitive function (S) and the complementary sensitive function (T), for all possible plants regarding uncertainties.

The transient behaviour is presented in Fig. 7, as the system step response for all the possible plants with the designed controller. All responses do not show important overshoot and they converge to the desired set-point. Also, the controller did not render any of the possible plants unstable.

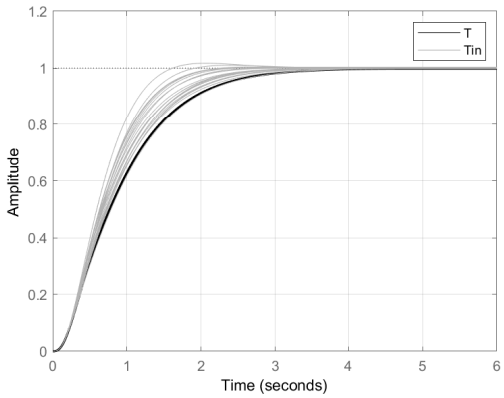

Figure 7. System step response for the nominal (T) and all the possible plants (Tin).

4.2 Simulation Conditions

The simulations were performed with the complete non linear system described in Sec. 2.2. The initial conditions for each of the following simulations is presented in Table 4.

Table 4. Initial conditions for simulations.

Parameter	Value
Stall speed – V_s	8.51 m/s
Straight flight velocity – V_{cr}	12.76 m/s
Climb velocity – V_{cl}	10.21 m/s
Initial altitude – h_0	0 m (sea level)
Static margin – SM	10%

The simulations occur at sea level conditions. The straight flight velocity was set at a value 50% above the stall speed,

whereas the climb occurs with a velocity 20% greater than V_s. The aircraft weight is set at its maximum value $W_{\mathbf{max}}$, presented in Table 1. All simulations were conducted with the complete non linear longitudinal model.

4.3 Simulation of the Response to an Elevator Doublet

To observe the differences in dynamic behavior for both the open and closed-loop systems, the aircraft is excited by an elevator doublet. Starting from a steady climb condition, a fast doublet input signal with a 5° amplitude and one second semi-period is applied over the elevator deflection at the trim condition. The responses are shown in Fig. 8, for the angle of attack (α) and pitch rate (q).

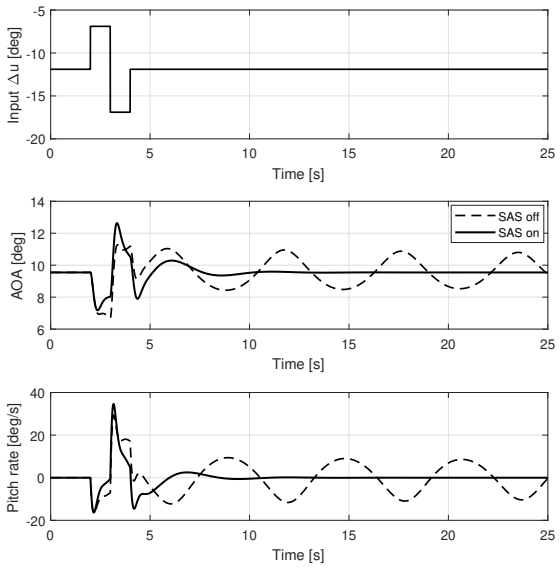

Figure 8. Short period response to an elevator doublet: angle of attack (AOA) and pitch rate (q).

The open-loop system (SAS off) continues to oscillate after the doublet is applied, whereas the closed-loop system (SAS on) quickly damps the oscillation, returning to the equilibrium values.

4.4 Simulation of an Attitude Change and Climb

An attitude change is simulated to show how the aircraft behaves when going from a straight and level flight to a climb condition with an abrupt control input. The altitude change can be seen in Fig. 9, with notable differences in dynamic behavior for both the open and closed-loop system ("SAS off" and "SAS on", respectively).

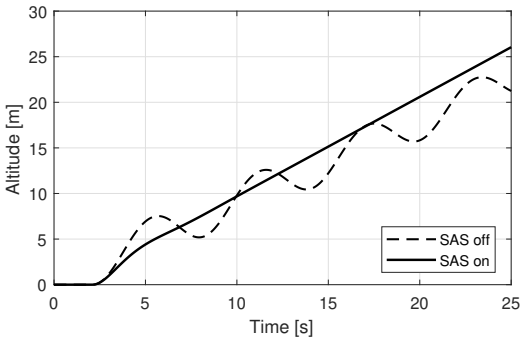

Figure 9. Altitude along the climb trajectory.

Starting from a straight and level condition with V_{cr}, at sea level, a step input is applied on the elevator at $t = 2\ s$, and the throttle is gradually increased, as show in Fig. 10. The goal of this maneuver is to put the airplane in a climb with V_{cl}, at approximately 5° of flightpath angle. However, due to flying quality issues, the aircraft does not achieve a stabilized climb and starts to oscillate, as shown by the dashed line in Fig. 9. When the SAS is turned on, the airplane quickly reaches the steady climb.

The control histories are shown in Fig. 10. With the SAS turned off, the elevator deflection remains constant, as show by the dashed line. With the SAS on, the elevator position does not remain constant, as can be seen in the solid black line. The variations in the elevator deflection are due to the robust controller acting to damp the oscillations.

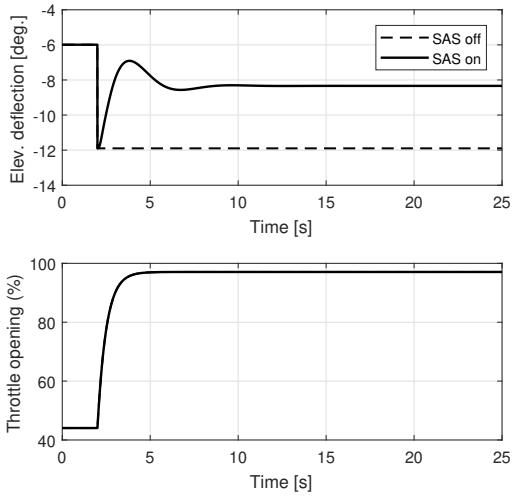

Figure 10. Elevator deflection and throttle opening along the climb trajectory.

The dynamic responses of the angle of attack and pitch rate to the maneuver are shown in Fig. 11. With the SAS off, the aircraft continues to oscillate after the control inputs are applied, whereas when the SAS is on, the oscillation is quickly damped and the vehicle stabilizes at the equilibrium values.

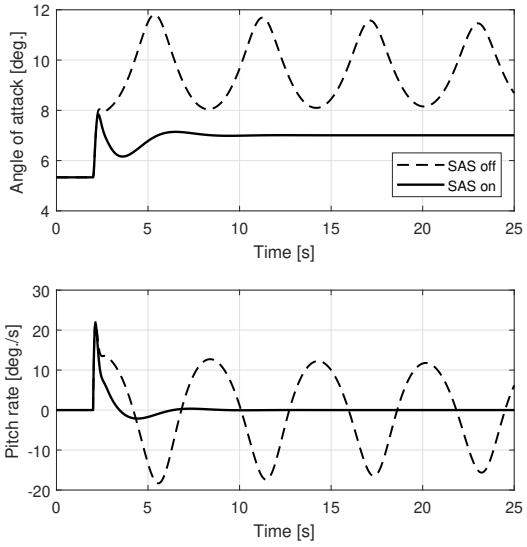

Figure 11. Angle of attack and pitch rate along the climb trajectory.

The dynamic responses of the true airspeed V and flightpath angle γ to the maneuver are shown in Fig. 12. With the SAS off, V and γ oscillate after the control inputs are applied, whereas when the SAS is on, the vehicle quickly stabilizes at the equilibrium values.

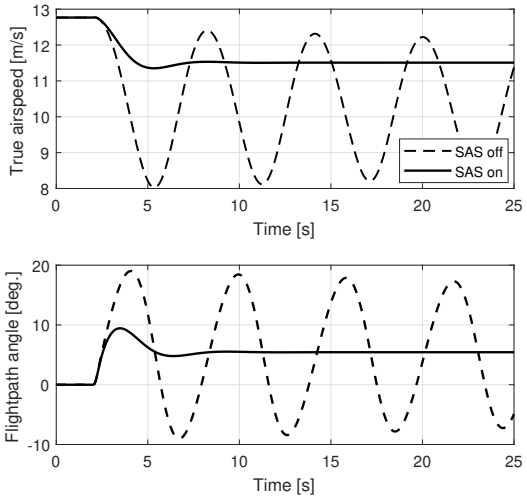

Figure 12. True airspeed and flightpath angle along the climb trajectory.

The aircraft oscillatory behavior reflects poor stability qualities, and can cause problems. If the oscillations reach large amplitudes, the aircraft may stall. The pilot will have to continually act upon the controls in order to damp the oscillations and prevent the aircraft to reach excessive angles of attack. This condition increases the pilot workload, and is detrimental to flight safety. As can be seen in the simulations above, the robust SAS is effective in dampening the oscillations and improving flying quality.

5. CONCLUSIONS

This work has presented the conceptual design of a robust longitudinal stability augmentation system aimed at improving aircraft flying quality. The robust design was conceived to deal with parametric uncertainties associated with the aircraft aerodynamic coefficients. In order to achieve robustness, the H_∞ technique was employed on the linearized short period approximation. Simulations were presented, showing both the open and closed-loop system dynamic responses to different inputs. It was concluded that the controller was effective in improving the aircraft stability and was able to keep good robustness, stability, and performance for all the uncertainties considered in the model. For future works, different models for actuator and sensor will be investigated, and the controller will be implemented in an actual airplane for flight tests.

ACKNOWLEDGEMENTS

This study was financed in part by the Coordenação de Aperfeiçoamento de Pessoal de Nível Superior – Brasil (CAPES) – Finance Code 001.

REFERENCES

Duke, E.L., Antoniewicz, R.F., and Krambeer, K.D. (1988). Derivation and Definition of a Linear Aircraft Model. Technical Report "NASA Reference Publication 1207", National Aeronautics and Space Administration.

Etkin, B. and Reid, L.D. (1996). *Dynamics of Flight: Stability and Control*. Wiley, Hoboken, NJ, third edition.

Jatengaokar, R.V. (2006). *Flight Vehicle System Identification*. American Institute of Aeronautics and Astronautics, Reston, VA, first edition.

Kannan, N. and Bhat, M.S. (2005). Longitudinal Hinfinity Stability Augmentation System for a Thrust Vectored Unmanned Aircraft. *Journal of Guidance, Control, and Dynamics*, 28(6), 1240–1250.

Keane, A.J., Sóbester, A., and Scanlan, J.P. (2017). *Small Unmanned Fixed-wing Aircraft Design: A Practical Approach*. Wiley, Hoboken, NJ, first edition.

Lombaerts, T.J.J., Mulder, J.A., Voorsluijs, G.M., and Decuypere, R. (2005). Design of a Robust Flight Control System for a Mini-UAV. In *AIAA Guidance, Navigation and Control Conference and Exhibit*.

McFarlane, D.C. and Glover, K. (1990). *Robust controller design using normalized coprime factor plant descriptions*, volume 138. Springer.

Nelson, R.C. (1989). *Flight stability and automatic control*. McGraw-Hill, New York, NY, first edition.

Peters, M. and Andrisani, D. (1997). The determination of longitudinal flying qualities requirements for light weight unmanned aircraft. In *AIAA Guidance, Navigation, and Control Conference*. doi:10.2514/6.1997-3701.

Skogestad, S. and Postlethwaite, I. (2007). *Multivariable Feedback Control: Analysis and Design*. Wiley-Interscience, Hoboken, NJ, second edition.

Stevens, B.L. and Lewis, F.L. (2003). *Aircraft control and simulation*. John Wiley & Sons, Hoboken, NJ, second edition.

Zhou, K. and Doyle, J.C. (1998). *Essentials of Robust Control*, volume 104. Prentice Hall, Upper Saddle River, NJ.

A Robust Longitudinal StabilityAugmentation System for Small AircraftUnder Parametric Uncertainty

Carta resposta

Gostaríamos de agradecer ao Editor Assossiado e aos revisores por seus comentários construtivos e avaliação detalhada do nosso trabalho. A carta de resposta foi montada de forma a responder os questionamentos feitos pelos revisores. Essas respostas se encontram abaixo com o texto escrito em azul.

Revisor 1:

1. Could the authors make the paper contribution clearer in the introduction?

A contribuição do artigo é mostrar o desenvolvimento de um sistema de aumento de estabilidade robusto simples e de baixo custo. Isto é descrito ao longo do texto. Infelizmente não há espaço para acrescentar mais um parágrafo no artigo.

2. Some illustrative Figures in Section 2 would be nice to illustrate the lift and drag forces and their relations with angle of attack as well as the CG.

Não foram incluídas mais figuras devido ao pequeno espaço disponível para o artigo.

3. I guess that pilot aggressive maneuvers are not allowed to avoid crashing due to modeling errors. Could the authors explore such issue in the paper?

Manobras (inputs de controle) não são categorizadas como incertezas de modelo. De fato, para qualquer aeronave, manobras agressivas não são permitidas durante testes iniciais. Se a aeronave estiver voando a altitudes muito baixas, manobras agressivas são sempre evitadas, exceto em casos de demonstração de acrobacias.

4. In the simulations, did the authors consider the linear approximate model or the simulations are carried out considering the nonlinear (and more precise) model

O projeto para o controlador robusto é realizado utilizando-se o modelo linear (Figuras de 4 a 7). Todavia, para o teste do controlador, foi realizadas simulações com o modelo não-linear (Figuras de 8 a 12). O texto ao final da seção 4.2 foi modificado para explicar isso.

Revisor 2:

1. As referências utilizadas são bastante antigas, citar referências mais atuais, pois o tema está bastante em voga.

As referências citadas ao longo do texto são as que foram utilizadas no projeto. Embora haja referências mais recentes na área de controle robusto, elas não foram utilizadas, e os autores não consideram correto neste caso citar trabalhos que não foram lidos.

2. Pequenos erros ortográficos ou de digitação.

O artigo foi novamente revisado de forma a corrigir estes erros.

Revisor 3:

1. Os testes em malha fechada com o controlador H_∞ projetado, realizados com diferentes representações lineares do sistema, conforme o conjunto de incertezas paramétricas definido na Tabela 2, permitiram a sua análise robusta a posteriori. Em outras palavras, a robustez em relação às incertezas paramétricas da Tabela 2 não é garantida a priori pela técnica de projeto.

O comentário é pertinente e este detalhe foi acrescentado ao texto com sua devida explicação.

2. Cabe salientar que apenas quatro parâmetros da Tabela 2 influenciam de fato as matrizes incertas A e B.

De fato, apenas quatro derivadas impactam o projeto do controlador. A tabela com as derivadas foi modificada, e as que não impactam o projeto do controlador robusto tiveram suas incertezas zeradas. O texto logo abaixo da tabela 3 também foi modificado para esclarecer isto.

3. O uso de letra D para indicar dois parâmetros distintos pode confundir o leitor (equações 2 e 14).

De fato, a escolha não foi adequada. As letras utilizadas para os parâmetros do atuador foram alteradas para eliminar a repetiçao e o risco de confusão.

4. Na Introdução não há citações relativas a trabalhos similares.

O último parágrafo da introdução foi substituído com uma comparação com os dois trabalhos mais próximos. Infelizmente o espaço é limitado e só foi possível incluir esses dois. Alguns trechos do texto precisaram ser alterados ou suprimidos para abrir espaço a esta alteração.

Revisor 4:

1. O trabalho está tecnicamente correto e bem escrito. Não existe nenhuma grande inovação do ponto de vista da teoria do projeto de controle, entretanto a aplicação é relevante, mesmo o trabalho apresentando apenas resultados de simulação. Como sugestão, em trabalhos futuros, os autores poderiam considerar representar o sistema não linear através de modelos fuzzy Takagi-Sugeno. Por fim, algumas siglas foram definidas mais de uma vez ao longo do texto e nas Equações (15) e (16) não vejo a necessidade de usar $\cdot$ para indicar a multiplicação.

Agradecemos os comentários e essas pequenas alterações foram adicionadas ao texto.

Revisor 5:

1. It should be clarified the advantages of the adopted control design technique in comparison with more recent approaches in the literature. What are the benefits of the adopted control technique when compared with more recent robust control techniques, e.g. the structured controller synthesis technique currently implemented in the SYSTUNE routine of Matlab, introduced in P. Apkarian, M. N. Dao and D. Noll, "Parametric Robust Structured Control Design,"in IEEE Transactions on Automatic Control, vol. 60, no. 7, pp. 1857-1869, July 2015?

Esta técnica de controle foi escolhida devido a sua simplicidade. Técnicas mais modernas apresentam algoritmos mais complexos e procuramos uma abordagem mais simples para o projeto. Todavia, é interessante, para trabalhos futuros, a camporação entre complexidade e desempenho entre os controladores.

2. On the other hand, since the various parametric uncertainties are handled via a single unstructured uncertainty, one should expect conservative results. That point was not discussed in the paper.

Realmente, os resultados obtidos através desta técnica, considerando o nosso tipo de incerteza, são conservadores. Este ponto foi adicionado ao texto.

3. Also, the adopted (full-order) control synthesis technique results in a 4th order controller for a 3rd order plant. Does the controller order represent an issue in the present application?

Não, a ordem do controlador não é importante neste caso. Entretanto, a observação é pertinente e abre espaço para uma investigação futura, a qual pode resultar em outro trabalho.

4. According to the text, Figures 6 and 7 depict responses "for all possible plants regarding uncertainties". How is it possible to obtain/depict system responses for the continuum of parametric values?

Para a obtenção dessas respostas utilizamos a ferramenta *ureal* do software Matlab. Esse comando permite escrever uma variável como incerta e colocar sua faixa de variação (no nosso caso, porcentagem). Ao realizar a simulação, o Matlab considera diversos valores para as incertezas além de seus valores extremais e nominal. Sua representação das várias possibilidades de se escrever o sistema (devido às incerteza) é mostrada pelas diversas linhas que aparecem nos gráficos dessas figuras. Essa simulação foi realizada diversas vezes em dias distintos e computadores distintos de forma a se verificar se haveria mudanças na resposta devido a valores diferentes de porcentagem da incerteza que o Matlab poderia considerar (nota-se aqui os valores intermediarios, os extremais e nominal sempre são considerados pelo Matlab). Como todas as simulações apresentaram o mesmo padrão de resposta (mesmo *shape*) consideramos o termo *for all possible plants regarding uncertainties* por ter sido observada uma ampla gama de possibilidades de simulações e em nenhuma delas ocorreu um resultado inesperado.